「森林総合研究所研究報告」（Bulletin of FFPRI），Vol.2, No.2（No.387），93-109, June, 2003

論文（Original Article）

SEM-EDXA study on the interface between wood and cement in Cement Strand Slab

FUJII Tomoyuki[1)]* and MIYATAKE Atsushi[2)]

Abstract

A new wood and cement composite named cement strand slab (CSS) has been developed to provide high mechanical and fire retardant properties. Focusing on the ultrastructure of the interface between wood and mortar, namely the mixture of cement, sand and water, in the CSS, this study investigated the distribution of chemical elements with an energy-dispersive X-ray analyzer equipped on a scanning electron microscope (SEM-EDXA). CSS samples were sub-carbonized in an oven with nitrogen-gas flow, and wood strands became brittle to prepare cross sections flat enough for SEM-EDXA investigation. Mortar was apparently filling tracheid lumina in the outermost layer of each wood strand and extended to a few layers inside. The composition ratio of Ca/Si in this region generally increased to 4-5 from around 2 in the ground mortar. The mortar in the outermost tracheid lumina was mostly rocky in appearance, similar to the adjacent mortar matrix. Some tracheids inside were filled with needle-like crystals that looked exactly like aggregations of chestnut burs. Occasionally, they were completely filled with mortar having a flat fractured surface and the Ca/Si ratio was always much higher than 100. Furthermore, wood strands in CSS were completely burned out to leave cinders of mortar molding tracheid lumina. It was obvious that mortar penetrated into and molded tracheid lumina. Within one tracheid, the molding mortar column transformed the texture from dense aggregates without apparent pores to diffuse aggregates of burs with long needles. Membranous cinder covering a column was observed and was continuous over adjacent columns. Therefore, the membranous cinder is probably derived from mortar that had penetrated into cell walls. They showed a high Ca/Si ratio of 13 to 30. As a result, we conclude that the physical continuity of mortar from ground matrix to those lumen-fillings provide the mechanical bonding between wood strands and ground matrix, and is reinforced by the deposition of Ca filling up cavities in aggregates of mortar.

Key words : Cement strand slab, CSS, SEM-EDXA, wood and cement composite, mortar, structure

INTRODUCTION

Fast-growing trees have been gaining attention as renewable resources rapidly in the last decade due to greater awareness of global environmental problems. Small-diameter stems or shoots from fast-grown trees and also waste wood from sawmills were split into strands with a roll press-slitter, and then the strands were bonded with common glue to produce a new wood composite called Superposed Strand Timber (SST), whose mechanical and strength properties are suitable for structural members (Fujii and Miyatake 1993, 1994a, Fujii et al. 1994b).

Wood strands were further applied to develop a new composite with mortar called Cement Strand Slab (CSS) at the Forestry and Forest Products Research Institute to provide high mechanical and strength properties. The CSS was evaluated to have enough strength and fire retardant for the structural members in house construction (Miyatake et al. 2000). As the modulus of ruptures (MOR) was improved by treatment with cement solution and affected by vacuum-pressure treatment with water, the contact between wood and cement was determined to be one of the most important factors affecting the strength of the composite.

Cement-bonded wood products are remarkably dependent upon species and their chemical compositions (Biblis 1968, Moslemi et al. 1983, Moslemi and Lim 1984). The interaction between wood and cement in those products has attracted an attention with interest since the 1970's and studied with a contemporarily developed scanning electron microscope (SEM) and also SEM equipped with an energy-dispersive X-ray analyzer (SEM-EDXA).

Samples investigated in the previous studies, however, were not sufficiently qualified or controlled to investigate the

原稿受付：平成14年12月25日 Received Dec. 25, 2002　原稿受理：平成15年３月11日 Accepted Mar. 11, 2003

1)* Department of Wood Properties, Forestry and Forest Products Research Institute (FFPRI), 1 Matsunosato, Tsukuba City, Ibaraki 305-8687, Japan; e-mail : tfujii@ffpri.affrc.go.jp

2) Department of Wood-based Materials, Forestry and Forest Products Research Institute (FFPRI)

This study was presented at the 48th and 49th Annual Meeting of the Japan Wood Research Society (Shizuoka, April 1998 and Tokyo, April 1999).

interaction.

Won and Moslemi (1980) observed a wood-cement composite with SEM. They attempted to relate the submicroscopic structure to strength development, but failed to show direct relationship between wood and Portland cement. Consequently, they assumed that mechanical interlocking plays a significant role and chemical forces are conceivably involved, and expected better sectioning techniques to facilitate a through examination of the wood-cement interface. In the recent serial studies on cement-bonded particleboard, Nagatomi et al. (1996a, 1996b, 1996c, 1996d) applied SEM and X-ray diffraction to investigate the crystal structure and the chemical composition of mineral educts of cement. The interface between wood-cement, however, has never been examined; only the fractured surfaces were investigated in the studies.

In contrast to the brittleness of cement giving more or less flat surface in fracture, woody elements are well known to be only rarely cracked transversely due to their peculiar cell wall structure. Particularly in the middle layer of the secondary wall (S_2 layer), cellulose microfibrils are dense and orientated parallel to each other in a steep helix to the fiber axis. It should be noted here that charcoal, carbonized wood, is brittle, and fractured cross sections are almost always flat, at least at the microscopic level. This suggests that carbonization or sub-carbonization of **CSS** will make the wood strands within **CSS** brittle enough to offer flat fractured surfaces. Furthermore, it is expected that full-combustion of wood strands within **CSS** will show micro-morphology of cement impregnated into wood in detail, as resin-casting methods applied to wood anatomy (Fujii 1993, Fujii and Hatano 2000) illustrated faithfully cell wall sculptures with polymer-casts remaining after the complete digestion of cell wall materials.

The present study focuses on the interface between wood and cement using SEM and on the topography of the chemical elements using SEM-EDXA. Neither crystalline structure nor eduction of mineral particles within cement is dealt with in this study, but impregnation of cement elements into macro- and micro-cavities within wood strands was examined to understand the contribution of the wood strands to the properties of CSS.

MATERIALS AND METHODS

Cement strand slabs (CSS)

The material used in this study was a part of the **CSS** examined for its mechanical properties, and the manufacturing process has been described in detail in a previous paper (Miyatake et al. 2000). The raw material consisted of Portland cement, **$CaCl_2$**, wood strands, sand and water. The chemical composition of Portland cement has some variation depending on the suppliers, but the general ratio as follows is well known (% in weight): CaO: 61-65, SiO_2: 20-21, Al_2O_3: 5, Fe_2O_3: 3, MgO: 1-2, SO_3: 2, Na_2O, K_2O & Cl: less than 1.

Outermost boards sawn from fresh logs of sugi (*Cryptomeria japonica* D. Don, Taxodiaceae: it is occasionally called by the name of Japanese cedar), plantation-grown in Miyazaki prefecture, Japan) were crosscut into 60 cm long pieces and then split twice into strands of 10 mm by 4 mm in cross section with a roll press splitter (Fujii and Miyatake 1993). The composition of **CSS** forming is shown in Table 1.

$CaCl_2$ was always added in water to 1 % of cement weight. The cement/sand ratio was twice as high in **CSS-b** as in **CSS-a** so that the water composition was increased. Wood strands were water-soaked and were orientated parallel to each other in the longitudinal axis of the **CSS**. After 2-days press, the **CSS** were cured for one month at room condition.

Sample preparation for SEM

The cross sections of dry wood strands were finished by sectioning with a sliding microtome equipped with a disposable knife (Feather S-35) (**Sample a**).

After a longitudinal bending strength test of **CSS-a**, fractured parts were crosscut with a diamond saw into about 1 cm long (Fig. 1). Longitudinal fractured surfaces including wood strands and mortar, namely the mixture of cement, sand and water, in a flat plane were sampled (**Sample-b**). Cross sections showing smooth fractured surfaces were much less frequent than the longitudinal ones. Only such areas where the cross sections of wood strands were at the same level as the surrounding mortar were sampled (**Sample c**).

Some pieces of CSS-b were sub-carbonized in order to make wood strands weak and brittle. They were heated in an oven in a nitrogen-gas flow up to 250 °C in 20 min. and kept between 250 and 300 °C for 90 min. The sub-carbonized CSS was broken easily by hand giving occasionally smooth surfaces including cross sections of wood strands at the same level as the surrounding mortar (**Sample-d**).

Some small pieces of sub-carbonized CSS (**Sample-d**) were heated with a flame, and wood strands were completely burned

Table 1. Samples

Sample	Comosition in ratio					Press	Density
	Strand	Cement	Sand	Water	CaCl2	MPa/sq.cm	g/cub.cm
CSS-a	3	4	4	2	0.04	2.3	1.48
CSS-b	3	5.3	2.7	2.7	0.05	2.3	1.4

leaving only mortar as cinders (**Sample-e**). From some of them, minute cinders resulting from the combustion of wood strands were transcribed on a carbon adhesive tape (**Sample-f**).

SEM-EDXA: Scanning electron microscopy with energy-dispersive X-ray microanalysis

The **CSS** samples for SEM were fixed with photo-glue (vinyl acetate) on one end of copper (**Cu**) tape adhered on a SEM stub so as to adjust the orientation by bending the **Cu**-tape. They were coated with **Pt-Pd** (80:20) in an ion-sputter coater (Jeol JFC-1100) at 1.5 keV with an electron current of 15 mA for 3 min. The **Pt-Pd** coating was preferred to carbon or gold for observation at higher resolution. Essentially, specific X-rays from **Pt** and **Pd** do not overlap in the energy levels with those of chemical elements expectable in **CSS**, although they may increase the background noise.

The samples were investigated within a SEM (Jeol JSM-840) equipped with an EDXA system (Jeol Super Mini-cup) and analyzed with a personal computer system (Jeol JED-2110 ver. 1.14). Micrographs of secondary electron images were taken at an accelerating voltage of 5 keV, and EDXA was carried out at 20 keV for spectrum analyses and element mapping (256 by 256 pixels).

RESULTS AND DISCUSSION

Sugi strand (Sample-a)

Wood strands of sugi manufactured with a roll splitter were roughly rectangular in cross section, and they had various large and small cracks along with growth ring boundaries and also in radial and diagonal directions irregularly (Fig. 2), and sometimes were torn into narrower strands with random shapes. Most tracheids on the longitudinal surfaces showed mainly the outer layers of the secondary walls (S1 layer), suggesting intra-wall fracturing, with occasional oblique-transverse fractures or tears showing apparent openings of the lumina (Fig. 3). The explanation of the process is that the roller splitter compressed laterally wood tissues with circular blades and mostly split and partly cut tracheid walls. As a result, tracheids on the lateral surfaces of the strands showed fractured surfaces caused by commonly ruptured and partly amputated parts that remained more or less tubular.

Longitudinal fracture surfaces of CSS (Sample-b)

Wood strands were easily distinguished from mortar by their appearance in a SEM, but the boundaries between them were not obvious. For example, Fig. 4 shows a boundary between a wood strand (right) and mortar (left). A tracheid lumen in the center (asterisk) was filled with mortar, but some others nearby on both the left and right sides (arrow heads) were empty. The impregnating depth of mortar into wood was not apparent here, because it was very hard to distinguish tracheid walls, whether they were on the original surfaces of the wood strand or on the fractured surfaces caused by the sample preparation for the SEM study.

Furthermore, the boundary was not expectable to be so adequately perpendicular to the surface that it was very hard to determine whether mortar beneath tracheid walls are those filling tracheid lumina or the outermost part of mortar matrix. To avoid such misunderstanding, further investigation was carried out using cross sections.

Cross surfaces of CSS (Sample c and d)

Flat surfaces including both cross sections of wood strands and mortar matrix were occasionally obtained on the tension side of bending-test samples (**Sample c**, Fig 1). But, they rarely offered flat planes suitable for SEM-EDXA. **Sample d** (obtained through sub-carbonization) appeared similar to **Sample c** under SEM observation, and no distinct characters were investigated between them as far as the boundary regions between wood strand and mortar are concerned. The difference was found only in the fracture surfaces of tracheid walls: they showed smooth cross sections in **Sample d,** but showed the three-layered structure of the secondary walls in **Sample c.**

The flat areas in **Sample d** were enough wide for the SEM-EDXA investigation on the relationship between mortar and wood strands (Fig. 5). Most gaps or cracks in wood strands were completely filled with mortar (Figs. 6 & 7), but some were apparently empty. Such empty cracks are believed to be artifacts caused by the considerable shrinkage of wood during the sub-carbonization process confronted with rigid mortar matrix. Also, wood strands were often fractured transversely at a different height-level to mortar matrix, leaving the peripheral parts attached on the mortar matrix. These facts suggest that wood strand and mortar should be tightly bonded with each other during **CSS** manufacturing.

No difference in structure of strand and distribution of mortar near the boundary was found in this study despite the conspicuous difference in water content of wood strands during **CSS** formation, such as air-dried or water-soaked.

On the fractured surface, every tracheid lumen in outermost layer of each wood stand was apparently completely filled with mortar (Figs. 7a, 8a & c). In a few layers inside, some were completely filled and others were partly filled or nearly empty. The composition and distribution (i.e., topography) of chemical elements in a wide area including wood strands and neighboring mortar matrix were analyzed by SEM-EDXA at low magnification (Fig. 6). The results were not considerably different between **Sample-c** and **Sample-d**, despite the fact that the latter was affected by the high temperature treatment (Table 2). Besides the **Pt** and **Pd** that were in the coating material for

SEM observation, the major elements detected were **C**, **O**, **Ca** and **Si.** Two of these elements, **C** and **O** were, remarkably affected by the occupation ratio of wood strand within an analyzed area (Compare SEI, **C and O** in Fig. 6). Minor elements detected were **Al, Fe** and **Mg**, and occasionally **Na**, K, **Cl** and **S** (Table 2). Mortar matrix was composed mainly of **Ca** + **O** and scattering particles were different in the composition as follows: **Si** + **O**, **Si** + **O** + **Al**, **Si** + **Al** + **O** + **K**, and **Si** + **Al** + **O** + **Na** (Fig. 6). Often higher concentrations of **Ca** were detected in the periphery of wood strands, therefore the heterogeneous distribution of this predominant element in the cement was evaluated with the composition ratio against **Si**, which is another major element. The ratio of **Ca/Si** was usually a little higher than 2, when a wide area was analyzed, but it commonly increased to 4-5 in the boundary region of about 0.1 mm wide between the matrix and wood (Table 2).

The mortar filling the outermost tracheids was rocky in appearance similar to that of the adjacent mortar matrix (asterisks in Figs. 8a & c). It can be attribute to the fact that the outermost tracheids were mostly ruptured during the splitting process to produce the strands and the lumina were open to the mortar matrix. The **Ca/Si** ratio mostly of 4-5 was higher than those of the mortar matrix (Table 2). Most unruptured tracheids in the second layer, at least in the cross section, were filled with mortar, and the distribution of **Ca** and **Si** were similar to those filling the outermost tracheids and the ground matrix (arrow

Table 2. Composition of chemical elements

Sample	Mag.*	Object	Chemical elements (% in weight)													**Ca/Si ratio**	Pd/Pt ratio
			C	O	Na	Mg	Al	**Si**	S	Cl	K	**Ca**	Fe	Pd	Pt		
Sample-d: Cross fractured surfaces of sub-carbonized CSS	20	Wide area	12.8	53.0	0.4	0.5	1.8	**7.2**	0.3	0.1	0.7	**16.1**	1.4	0.8	4.7	**2.2**	0.17
	100	Wide area	13.1	52.2		0.3	0.7	**7.1**	0.2		0.3	**15.2**	0.8	1.3	7.8	**2.1**	0.17
	100	Wide area	13.2	62.7	0.4	0.1	1.1	**2.9**	0.1		0.2	**4.8**	0.4	0.6	2.6	**1.7**	
	100	Wide area	17.4	57.0	0.4	0.3	1.7	**3.4**	0.2		0.2	**4.1**		2.3	12.7	**1.2**	0.18
	500	Boundary	7.5	43.5		0.5	1.0	**6.4**	0.4			**29.9**	1.3			**4.7**	
	1,000	Crack filling	15.7	55.1		0.1	0.7	**3.4**	0.2	0.2	0.4	**15.8**	0.7	1.1	5.6	**4.6**	0.20
	500	Rocky matrix	9.8	46.2		0.5	1.2	**5.2**	0.5		0.2	**24.4**	1.2	1.9	8.8	**4.7**	0.22
	500	Rocky matrix	9.8	46.2		0.5	1.2	**5.2**	0.5		0.2	**24.4**	1.2	1.9	8.8	**4.7**	
	500	Rocky matrix	11.6	47.3			0.4	**1.1**			0.3	**35.0**	0.5			**31.8**	
	7,000	Rocky matrix	7.7	42.8		1.0	1.8	**3.7**	0.4	0.2	0.5	**31.6**	2.9	1.1	6.0	**8.5**	0.18
	17,000	Rocky matrix	8.4	42.2			0.4	**3.5**				**34.0**		2.8	8.6	**9.7**	0.33
	10,000	Aggregate of burs	15.5	54.3		0.4	0.9	**4.1**			0.5	**14.3**	0.9			**3.5**	
	10,001	Aggregate of burs	16.5	55.3		1.4	1.9	**5.1**			1.5	**15.3**	1.9			**3.0**	
	8,000	Dense aggrigate	10.0	61.6		0.4	0.5	**1.9**	0.2	0.1	0.2	**8.0**	0.8			**4.2**	
	2,000	Flakes in limen	8.2	50.5	1.0	0.5	6.5	**12.9**	0.3		0.9	**5.6**	5.5	1.1	2.7	**0.4**	0.41
	8,000	Flat lumen	7.0	37.8				**0.2**				**41.9**		2.2	10.8	**209.5**	0.20
	22,000	Flat lumen	7.8	39.7				**0.4**			0.4	**42.4**		1.5	7.4	**106.0**	0.20
Samples-e & **-f:** Cinders remaining after the combustion of CSS	140	Wide area	10.5	46.8	0.9	0.4	1.0	**3.7**	0.2			**28.0**	0.8	0.9	5.3	**7.6**	0.17
	500	Wide area	22.4	64.1	0.2		0.2	**0.9**			0.3	**4.6**	0.2	0.9	5.2	**5.1**	0.17
	12,000	Fe-Al grain	17.9	56.7	0.6	0.3	1.0	**1.2**	0.1		0.6	**9.4**	1.3	1.6	8.2	**7.8**	0.20
	10,000	Bur-like grains	23.2	66.2	0.1	0.2	0.3	**1.0**	0.1		0.2	**4.1**	0.2	0.6	3.1	**4.1**	0.19
	1,000	Granular to dense Columns	7.4	42.5	1.3	0.6	1.2	**5.6**	0.5		1.8	**28.7**	1.0	1.5	7.5	**5.1**	0.20
	8,000	Dense column	10.7	46.3	0.4		0.5	**1.7**	0.4		0.7	**33.3**		1.0	4.6	**19.6**	0.22
	700	Boundary	11.7	51.1	0.7	0.3	0.6	**8.8**			1.1	**17.1**	0.8	1.4	6.2	**1.9**	0.23
	19,000	Dense column	14.3	50.3				**0.1**	0.1			**25.5**		1.7	7.9	**255.0**	0.22
	19,000	Dense column	13.4	50.8	0.3	0.2	0.7	**3.7**	0.3			**19.4**	0.4	2.0	8.8	**5.2**	0.23
		Cell wall	24.9	68.3				**0.2**				**2.7**		0.6	3.2	**13.5**	0.19
	10,000	Cell wall	12.0	48.3	0.2	0.2	0.6	**2.6**	0.3			**26.4**	0.3	1.5	7.7	**10.2**	0.19
	10,000	Cell wall	22.2	62.7	0.9			**0.1**				**3.0**		1.5	8.5	**30.0**	0.18
	2,300	Cell wall	22.3	63.5	0.7		0.1	**0.2**	0.1		0.6	**4.3**		1.2	6.1	**21.5**	0.20
	8,000	Pit chamber	8.1	41.1				**0.4**	0.2			**43.8**		1.0	5.0	**109.5**	0.20
	18,000	Pit chamber	11.6	49.9	0.4	0.5	1.4	**6.1**	0.3			**21.1**	0.6	1.4	6.9	**3.5**	0.20
	18,000	Pit chamber	14.2	50.4	0.2	0.1		**0.6**	0.1			**24.8**		1.8	7.7	**41.3**	0.23
	10,000	Cell wall	22.7	63.7				**0.1**			0.1	**3.7**		1.4	7.3	**37.0**	0.19

*:Magnification directly regulates the area of the measurement.

head 1, compare **Si** and **Ca** in Fig. 8b). They were aggregation of needle-like crystals that looked just like chestnut burs (Fig. 8c). Occasionally, mortar filling tracheid lumina was conspicuously rich in **Ca** (arrow head 2 in Fig. 8b) and was not visible in **Si** map (Fig. 8b). They showed flat fractured surfaces (arrow head 2 in Fig. 8c). In the aggregation of needle-like crystals that looked just like chestnut burs, mineral elements such as **Ca**, **Si**, **Al**, **Fe**, **Mg** and **K** were detected at the same level as ground mortar (Table 2 and Fig. 9, compare Fig 9b with Fig. **7c**). The mortar showing the flat fractured surfaces, that were occasionally found in tracheid lumina and always completely filled them up, showed the **Ca/Si** ratio much higher than 100 (Table 2 and Fig. 10, compare Fig. 10b with Figs. 7c & 9b).

Cinders of wood strands in CSS

After wood strands in a small piece of **CSS** were completely burned out, cinders of the wood strands were left and appeared as piled-up logs remaining the original arrangement of the tracheids (Fig. 11). The columnar remnants arranged parallel to each other and inclined gently toward the mortar matrix (Fig. 12). They were mortar which had ever filled the tracheid lumina. Within a column, they were diffuse aggregate of bur-like grains at the top end. Then, the density of the aggregation increased toward the base of the column, and at the same time the length of the needles gradually decreased (Fig. 13). Finally, tracheid wall sculptures such as pit borders and pit cavities were apparently observed in some parts with fine texture (Fig. 14). It was obvious that the mortar, excluding sands, had penetrated into tracheid lumina for some depth from openings on the lateral surfaces and molded the tracheid shape. Within one tracheid, the mortar column transformed the surface texture from diffuse aggregate of burs to fine without apparent pores. As is apparent in Fig. 12, the diffuse aggregates were located deeper in each wood strand than the fine textured part. This means that the density of the mortar within each tracheid lumen usually decreases from the opening of the tracheid toward the tip.

Won and Moslemi (1980) mentioned that needle-like crystals, that had primarily been generated by the hydration of tricalcium silicate and tricalcium alminate, as well was smooth, conical, rock-like crystals that had formed as a result of the addition of calcium chlorite, appeared likely to interlock with tracheid wall surfaces and grow into whatever cavities were present there. These crystals may account for the greatest proportion of the strength of the composite. But, it is only a guess without any direct imaging. SEM micrographs prepared by complete removal of cell wall materials with combustion revealed that the surfaces of mortar molding tracheid lumina were smooth without any needle-like protrusions (Fig. 14). This suggests that the crystals could not butt against tracheid wall surfaces.

In SEM-EDXA there was some concern that the mortar matrix behind the tracheid molding mortar columns could injuriously affect the topochemical analysis, especially when thin membranous cinders or low-density aggregations of grains were targets. To get rid of the risk, cinders were transcribed on a carbon adhesive tape. In Fig. 15a, three columnar remnants are shown. The spectra taken from the whole area was almost the same as those from the mortar filling tracheid lumina in the sub-carbonized samples except for the high yields of C and **O** which came from the carbon adhesive tape in the background (Table 2, Fig. 15b compare with Fig. 7c). The top one showed the dense and fine texture, but showed the granular texture in the distributions of **Fe** and **Al** despite of the high concentration of **Ca** and **Si** (Fig. 15c). The middle one was the aggregates of grains and apparently morphologically different from the top one, but the topology of minerals such as **Ca**, **Si**, **Al** and **Fe** were similar to the top one. The bottom one was a set of membranous cinder showing the bordered pits structure, and the topochemical nature was not clearly illustrated here, because it was too low in the density to gain enough specific X-ray signals within the measuring condition suitable for dense remnants. The results on these membranous cinders are described later.

Among columnar cinders, abrupt morphological changes from fine and dense aggregates of grains to extremely fine texture without apparent cavities were occasionally found (Figs. 16a & 17a). The abrupt changes in the composition from **Ca** + **Si** to predominantly **Ca** occurred at the same part (Figs. 16b, 17b & c). The **Ca** predominant parts probably correspond to the mortar molding completely tracheid lumina and showing flat fractured surfaces in cross section. The **Ca/Si** ratios were extremely high in both cases (Figs. 8b & 16b, Table 2). It is still noteworthy that **Si** and other major elements were detected to some extent (Figs. 17c & 18b). Extremely high **Ca/Si** ratios were also recorded in mortar molding pit chambers (Figs. 18a & c, Table 2). These findings suggest that cavities within aggregates of grains are probably occupied subsequently with some substance predominated with **Ca**.

In some other parts, membranous cinders surrounded individual columns one by one and extended over adjacent columns (Figs. 19 & 20). In some cases, structure of pit borders was found (Figs. 21 & 22). They were sometimes fine in texture (Fig. 20) and sometimes granular (Figs. 21 & 22). These observations suggest that some part of mortar dissolved in water penetrated into cell walls to some extent, and the minerals of mortar dispersed within the cell walls condensed into small grains during the combustion of wood strands and were left as membranous cinders. The thin membranous cinders showed a somewhat high **Ca/Si** ratio of 10 to 30 (Figs. 22, Table 2), although it is not so high as dense and fine mortar molding

tracheid lumina, and the spectra were quite different from those from the aggregation of needle-like crystals (compare Figs. 22 with 23).

Conclusion

Based on the results of SEM and SEM-EDXA analyses in this study, we can concluded the formation and the mechanism of mechanical properties of the boundary between mortar matrix and wood strands as follows:

On the outer surfaces of wood strands, mortar always extended from the matrix to ruptured tracheid lumina. Therefore, the mortar in the outermost tracheid lumina was mostly rocky in appearance and having a little higher **Ca/Si** ratio similar to the adjacent matrix. Mortar in solution or in suspension passed through the lateral openings of tracheids into tracheid lumina for some longitudinal depth and aggregates of mortar were deposited densely near the base and sparsely around the tip. Subsequently, some solution predominated with **Ca** advanced into tracheid lumina and completely filled the cavities of the aggregates and those between mortar and cell walls only near the base.

Consequently, the physical continuity of mortar from the matrix to those lumen-fillings provides the mechanical bonding between wood stands and mortar matrix and is reinforced by the deposition of **Ca**-predominant substance filling cavities. Within the wood strands, the mortar molding tracheid lumina may have chemical and/or mechanical bonding with the mortar impregnated into tracheid walls. Such bonding may help to reinforce the anchor effect of the lumen-filling mortar, but it was not directly observed in this study.

REFERENCES

Biblis E. J. and Lo C. F. (1968) Sugar and other wood extractions effect on the setting of southern pine cement mixtures, Forest Prod. J., **18** (18), 28-34.

Fujii T. (1993) Application of a resin casting method to wood anatomy of some Japanese Fagaceae species, IAWA J. **14** (3), 273-288.

Fujii T. and Miyatake A. (1993) Manufacturing and properties of SST (Super Strand Timber) I. SST manufacturing from small-diameter logs, Abstract of the 43rd annual meeting of the Japan Wood Research Society, 552. (in Japanese)

Fujii T. and Miyatake A. (1994a) Manufacturing and properties of SST (Super Strand Timber) II. Properties of SST made from small-diameter logs, Abstract of the 44th annual meeting of the Japan Wood Research Society, 116. (in Japanese)

Fujii T. and Miyatake A. (1994b) Wood piled with split and disrupted pieces and its manufacturing method and manufacturing apparatus, European Patent Application, 94400191.6.

Fujii T. and Hatano Y. (2000) The LDPE resin casting method applied to vessel characterization, IAWA J., **21** (3), 347-359.

Miyatake A., Fujii T., Hiramatsu Y, Abe H. and Tonosaki M. (2000) Manufacturing of wood strand cement composites for structural use, in Proceedings of the 5th Pacific Rim Bio-Based Composites Symposium, Compiled by P.D. Evans, pp.115-118.

Molslemi A. A., Gorcie J. F. and Hofstrand A. D. (1983) Effect of various treatments and additives on wood Portland cement-water systems, Wood Fiber Sci., **15**, 164-176.

Moslemi A. A. and Lim Y. T. (1984) Capability of southern hardwoods with Portland cement, Forest Prod. J., **34** (7/8), 22-26.

Nagatomi W., Kuroki Y., Eusebio D. A., Ma L. F., Kawai S. and Sasaki H. (1996a) Rapid curing of cement-bonded particleboard II. Curing mechanism of cement with sodium hydrogen carbonate during steam injection pressing, Mokuzai Gakkaishi, **42**, 659-667. (in Japanese)

Nagatomi W., Kuroki Y., Eusebio D. A., Ma L.F., Kawai S. and Sasaki H. (1996b), Rapid curing of cement-bonded particleboard V. Mechanism of strength development with fortifiers and accelerators during steam injection pressing, Mokuzai Gakkaishi, **42**, 997-984. (in Japanese)

Nagatomi W., Kuroki Y., Kawai S. and Sasaki H. (1996c) Rapid curing of cement-bonded with silica fume I. Effects of an additive cement hydration during steam injection pressing, Mokuzai Gakkaishi, **42**, 1090-1097. (in Japanese)

Nagatomi W., Kuroki Y., Kawai S. and Sasaki H. (1996d), Rapid curing of cement-bonded with silica fume II. Effects of autoclave curing cement hydration, Mokuzai Gakkaishi, **42**, 1202-1210. (in Japanese)

Won Y. A. and Moslemi A. A. (1980) SEM examination of wood-Portland cement bonds, Wood Sci., **13** (12), 77-82.

セメント・ストランド・スラブにおける木材とセメントの界面の微細構造およびセメント成分の分布

藤井 智之*1) ・宮武 敦2)

要　旨

スギ・ストランドとセメントを原料としたスラブ（CSS）の製造条件と製品の性能評価において、内部構造を理解することが重要である。両者の結合状態を把握する目的で木材とセメントの界面付近の微細構造および成分の分布を走査電子顕微鏡－エネルギー分散型エックス線分析装置（SEM-EDXA）を用いて調べた。静的曲げ強度試験に供試したCSS試験体を窒素ガス環流条件で約80分間約250℃で亜炭化することにより木材ストランドを脆弱化し、割裂によりSEM-EDXAに必要な平坦な面を作製した。個々のストランドの表面の最外層にある仮道管の内腔はモルタルで充填され、さらにその内側の２－３層の仮道管にも広がっていた。最外層の仮道管内腔を充填するモルタルの形状は多くの場合、隣接する基盤モルタルと同様に岩状であった。この部分のモルタルのカルシウム（Ca）とケイ素（Si）の構成比率（Ca/Si比）はおおよそ４～５と、基盤のモルタルの約２から高くなっていた。内側の仮道管内腔にはイガ栗状の針状結晶が疎ないし密に集合していた。平滑な破断面のモルタルで充填された仮道管も稀に観察され、そのCa/Si比は常に100以上であった。さらに、CSS試料中の木材ストランドを炎中で灰化することにより、ストランド中のモルタルを残渣として取り出した。その形態および成分の分布状態からモルタルが仮道管の内腔に浸入し、内腔を充填していることが明らかとなった。個々の仮道管中では、モルタルは基盤に近い基部では空隙のほとんど見られない程までに粒子が高密度に凝集し、ストランド内方の先端に向かってその密度が減少していた。時には、Ca/Si比が100以上と著しく高く、かつ壁孔腔等の仮道管壁の立体構造を忠実に写し出している部分が観察された。仮道管内腔を充填する円筒状のモルタルを包み込み、さらに隣接仮道管まで連続するように広がった膜状のモルタルが観察された。そのCa/Si比は13～30であった。この膜状のモルタルは仮道管の細胞壁中に浸透していたものが細胞壁の灰化によって凝集したものと推察される。観察結果に基づいて、基盤からストランドの仮道管中へ物理的に連続するモルタルが木材ストランドと基盤モルタルを機械的に結合しており、さらに仮道管内腔を完全に充填するCa成分で強化されていると推察される。

キーワード：セメント・ストランド・スラブ、CSS、 SEM-EDXA、木質材料、モルタル、微細構造

1)* 森林総合研究所 木材特性研究領域　〒305-8687 つくば市松の里1 e-mail : tfujii@ffpri.affrc.go.jp
2)　森林総合研究所 複合材料研究領域

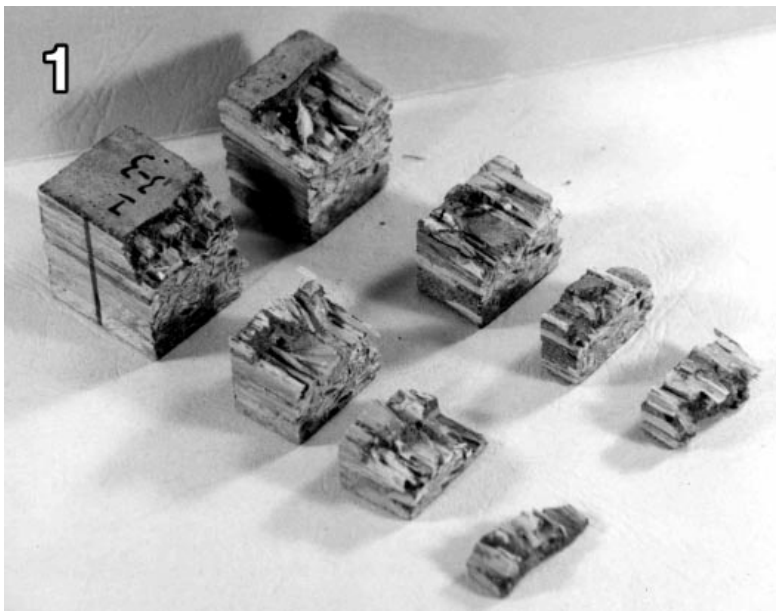

Fig. 1 After a longitudinal bending strength test, fractured parts of **CSS** were crosscut with a diamond saw into about 1 cm long.

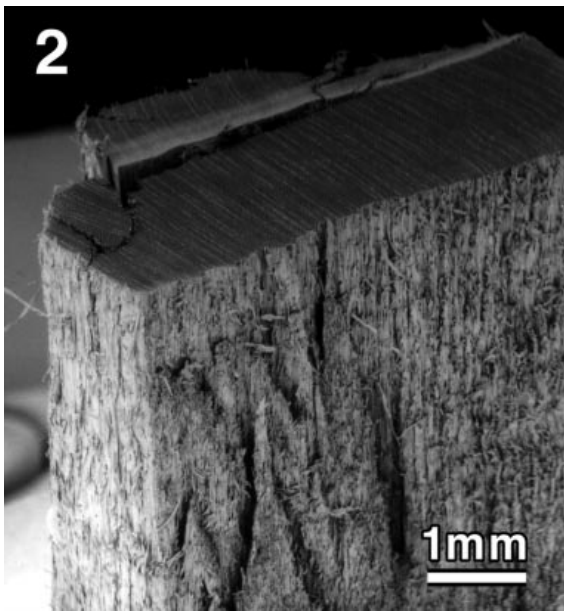

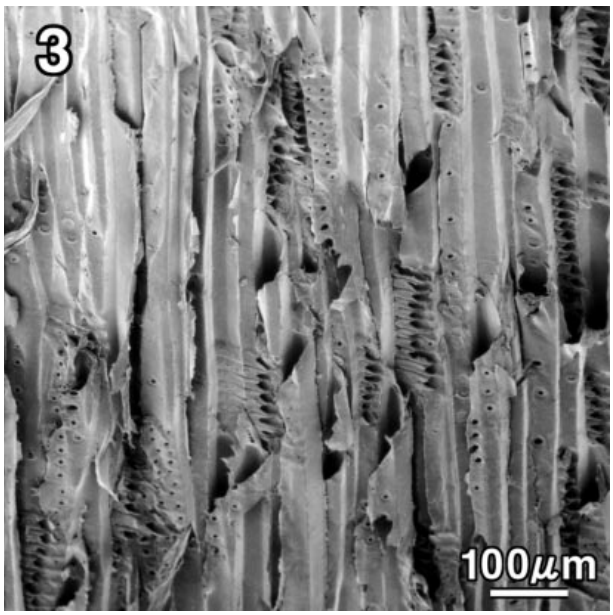

Fig. 2 Sample-**a**. Three-dimensional view of a sugi strand showing a cross section finished by microtome knife and split longitudinal surfaces.

Fig. 3 Sample-**a**. Oblique radial-longitudinal surface of the strand. Tracheids were split in lateral walls and torn-off longitudinally.

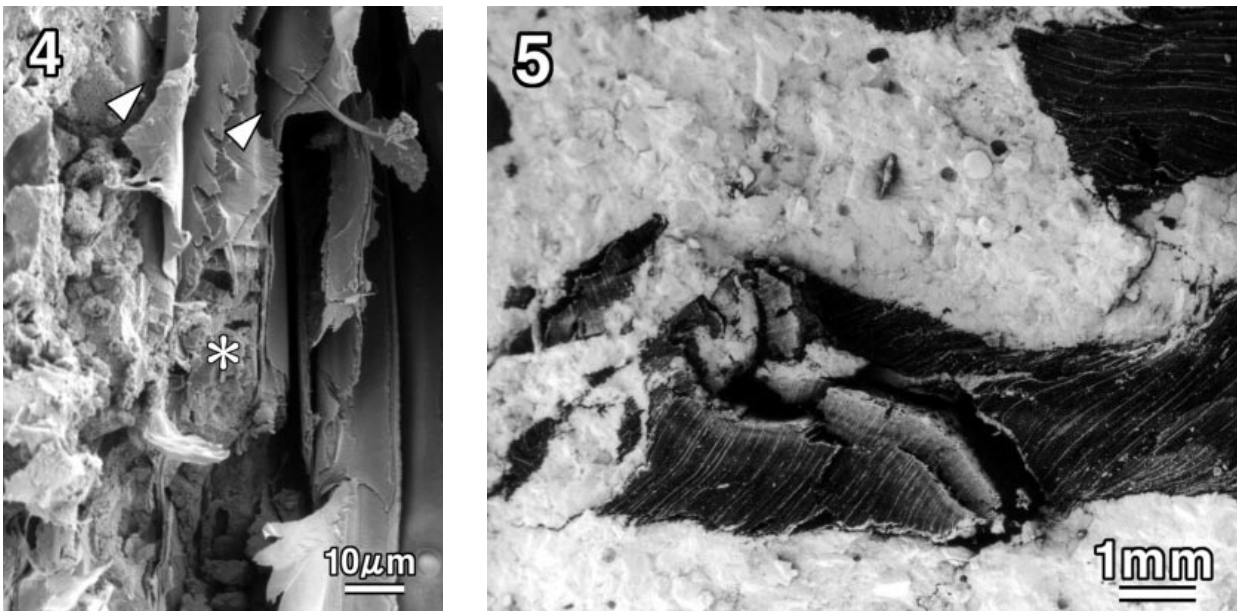

Fig. 4 Sample-**b**. Longitudinal fractured surface of **CSS** showing the boundary between wood strand and mortar. A tracheid lumen in the center (asterisk) was filled with mortar, but some others nearby on both the left and right sides (arrow heads) were empty.

Fig. 5 Sample-**d**. Cross-fractured surface of sub-carbonized **CSS**. Tangential cracks in wood strand are artifact caused by the deformation during sub-carbonization.

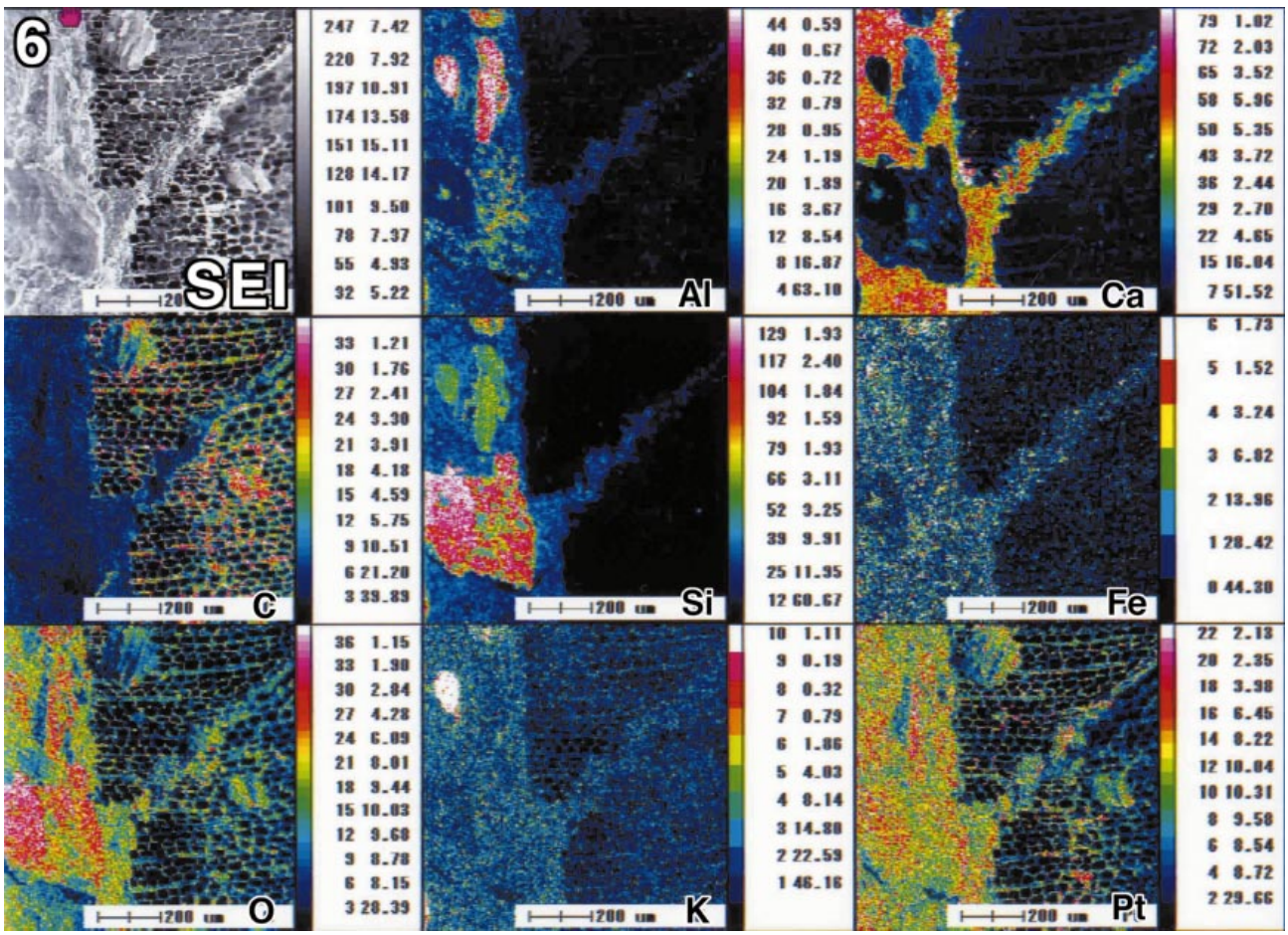

Fig. 6 Sample-**d**. Secondary electron image (SEI) and element maps at low magnification. Scattering particles rich in **Al**, **Si** and **K** are prominent as white to red dots in relevant maps. Take notice that the color gradations are different among the maps.

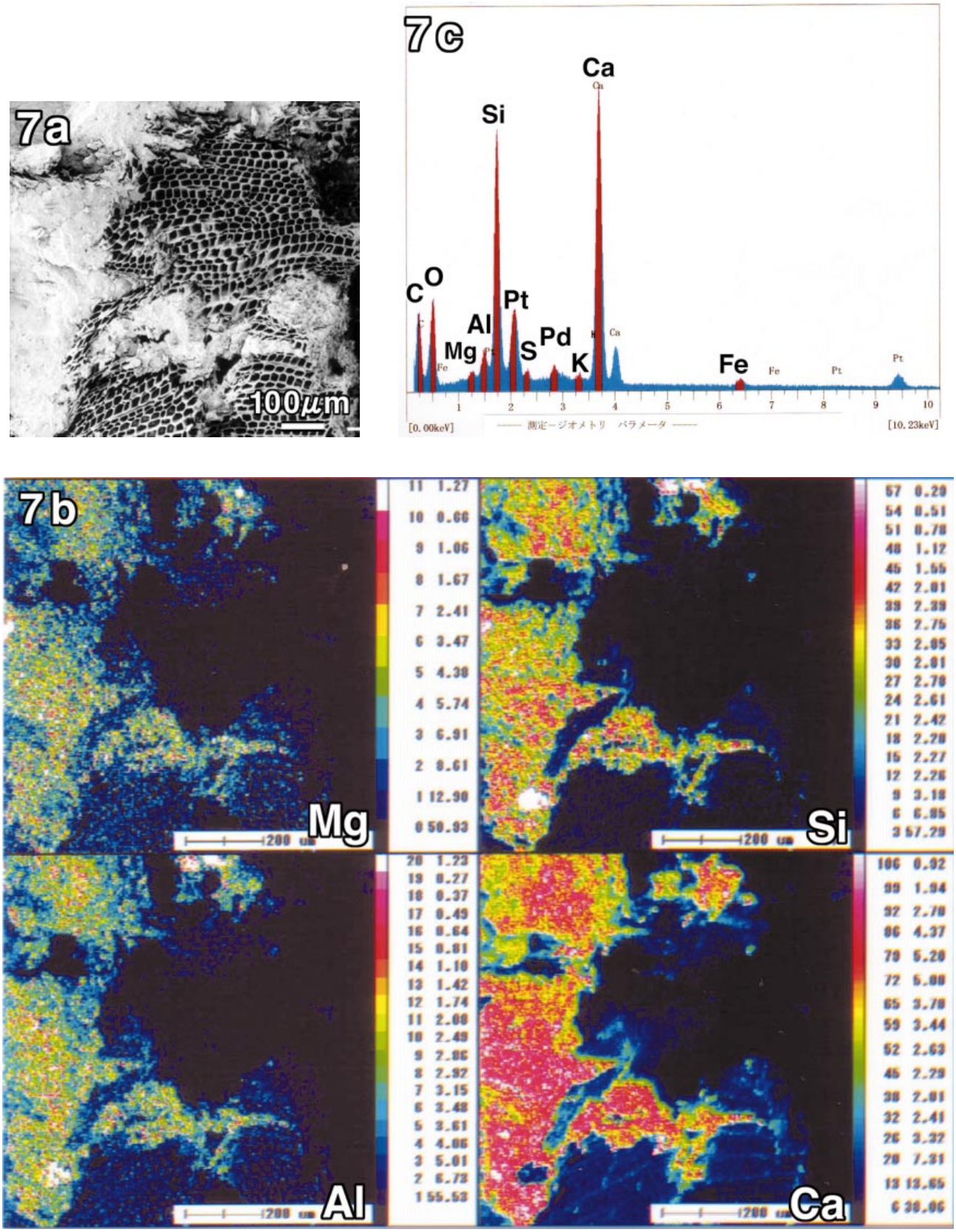

Fig. 7 Sample-**d**. Selected area from Fig.5. **7a**: SEI, **7b**: element maps of **Mg**, **Al**, **Si** and **Ca**, **7c**: EDS spectrum obtained from whole area of Fig. 7a. Cracks in the wood strand were completely filled with mortar, which chemical composition was similar to the ground matrix. Take notice that the color gradations are different among the maps.

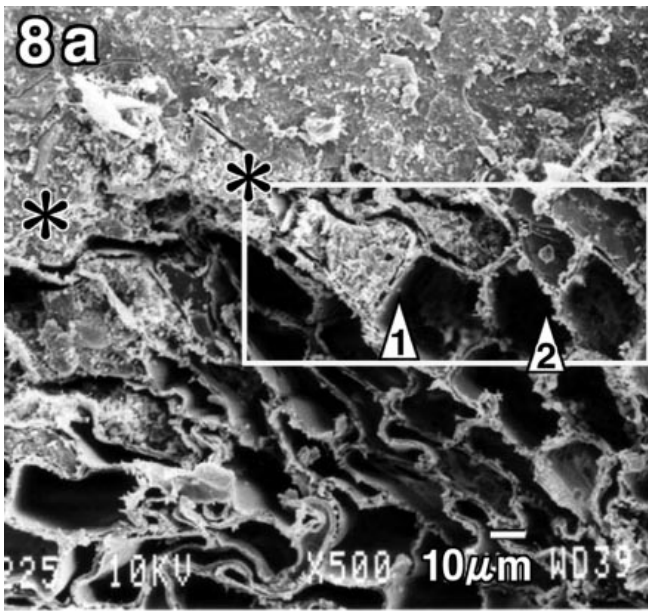

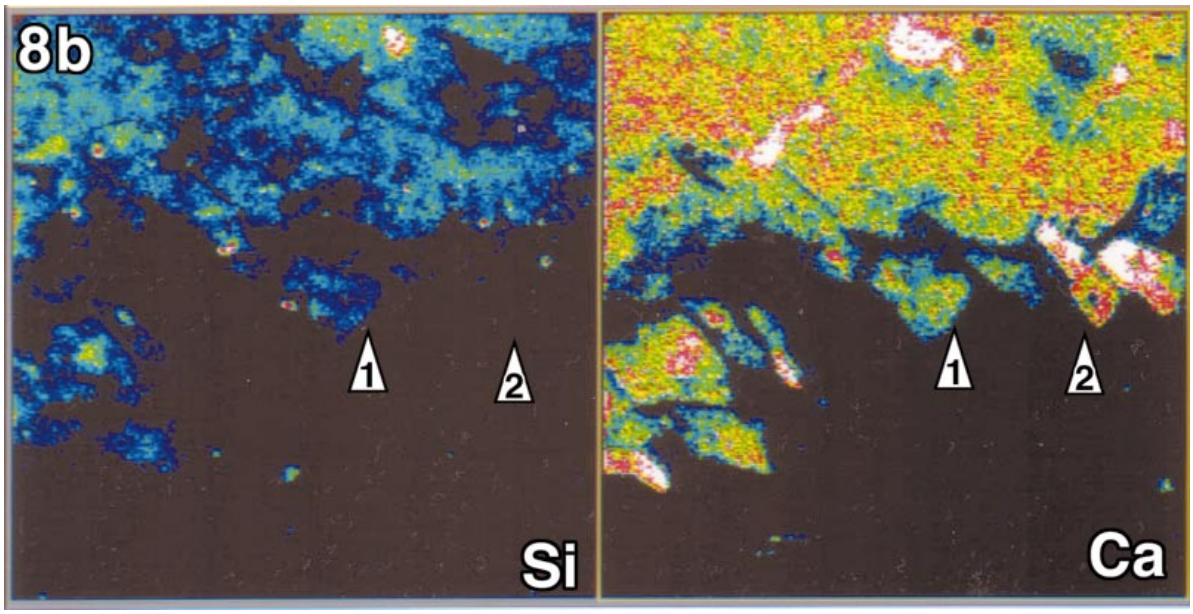

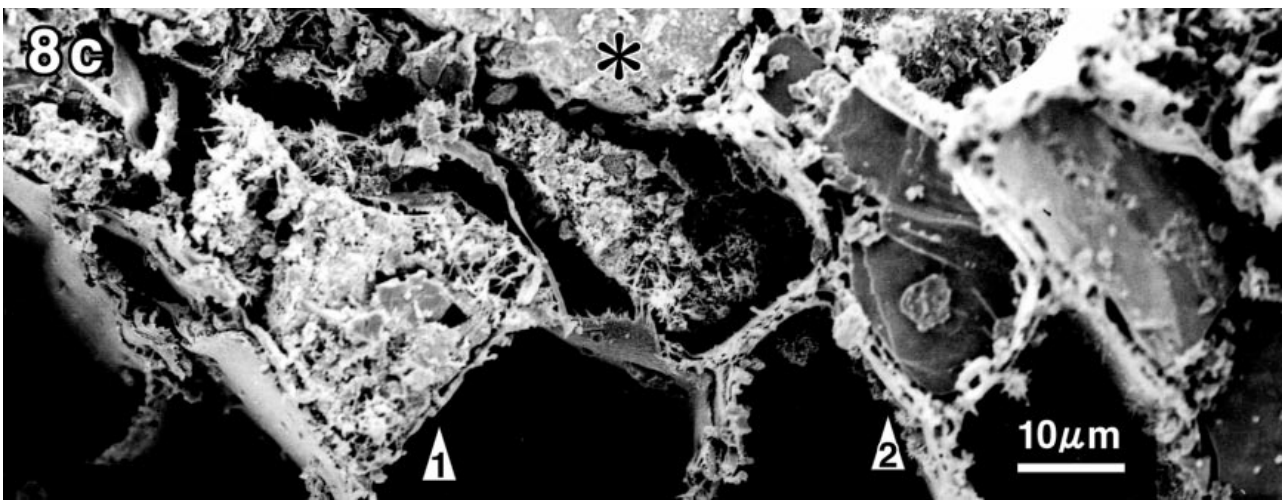

Fig. 8 Sample-c. **8a**: SEI, **8b**: element maps of **Si** and **Ca**. **8c**: SEI of the selected area from 8a. The mortar filling the outermost tracheids (*) was rocky in appearance similar to that of the adjacent mortar matrix. Most tracheids just inside were filled with aggregation of needle-like crystals and the distribution of **Ca** and **Si** were similar to that of ground matrix (arrow head 1). Occasionally, they were fractured in flat surfaces and conspicuously rich in **Ca** (arrow head 2).

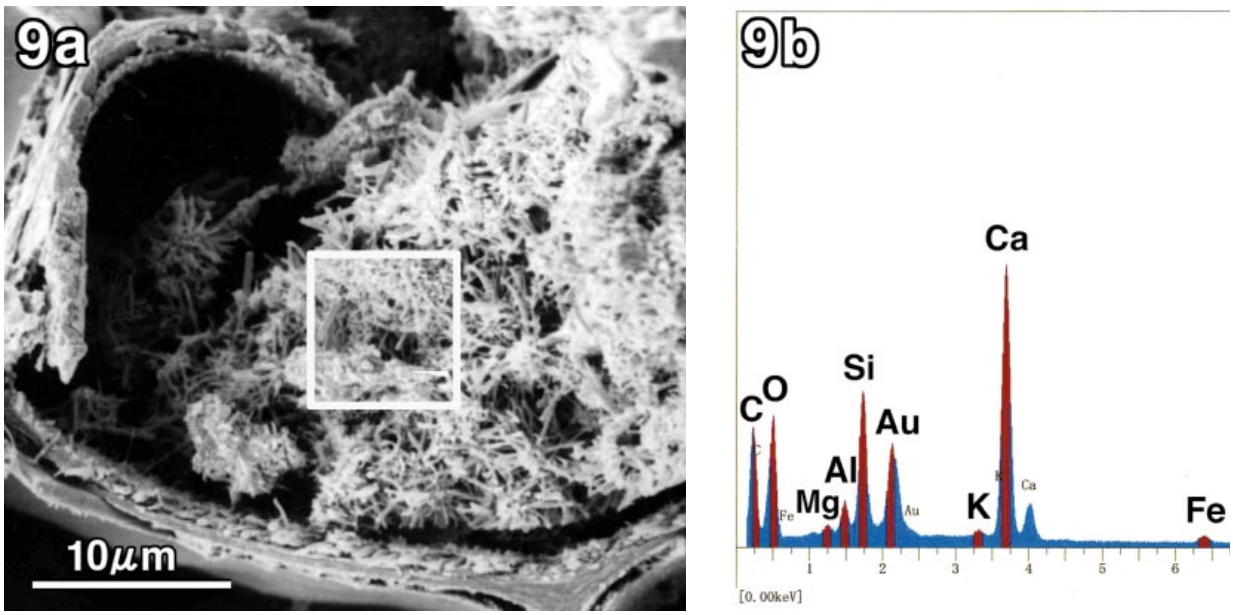

Fig. 9 Sample-**d. 9a**: SEI, **9b**: EDS spectrum of the enclosed area in Fig. 9a. In the aggregation of needle-like crystals, mineral elements such as **Ca**, **Si**, **Al**, **Fe**, **Mg** and **K** were detected at the same level as ground mortar.

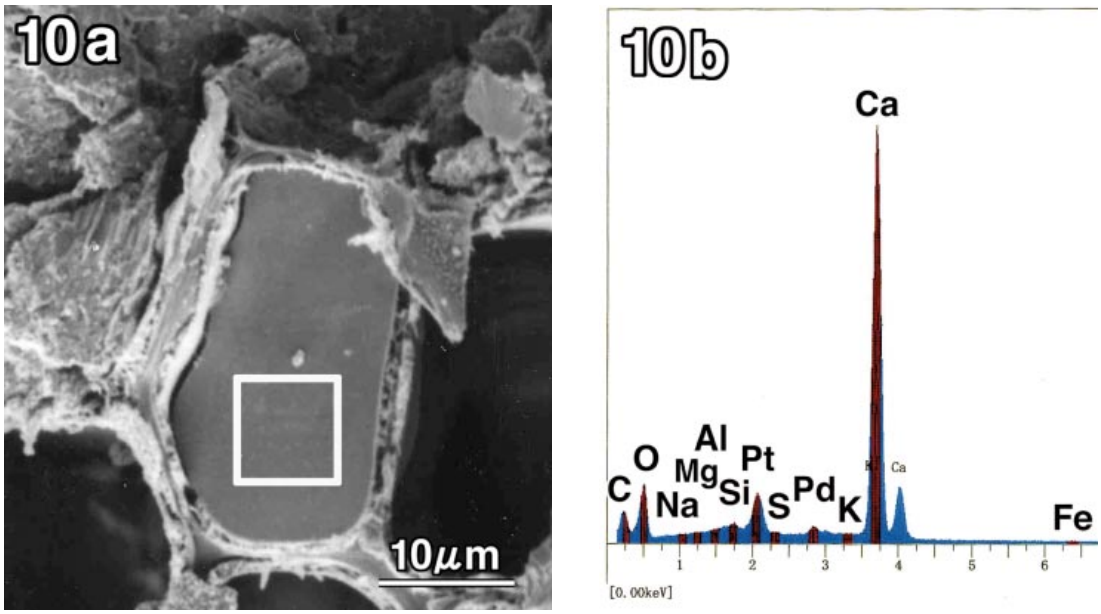

Fig. 10 Sample-**d. 10a**: SEI, **10b**: EDS spectrum from the selected area. Mortar showing the flat fractured surfaces always completely filled up a tracheid lumen and conspicuously rich in **Ca**.

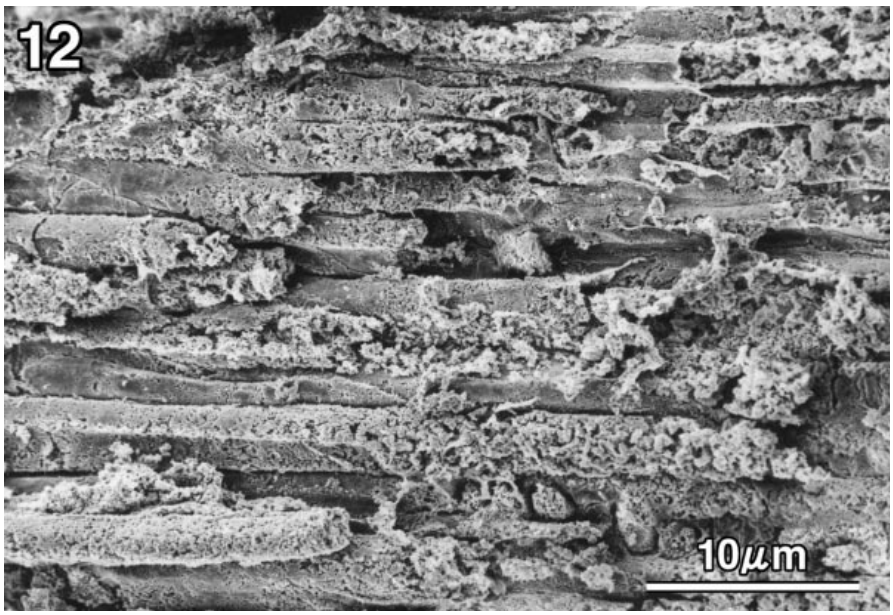

Fig. 11 Sample-**e**. A piece of **CSS** after combustion in a flame.
Fig. 12 Sample-**e**. Cinders appeared as piled-up logs remaining the original arrangement of the tracheids.

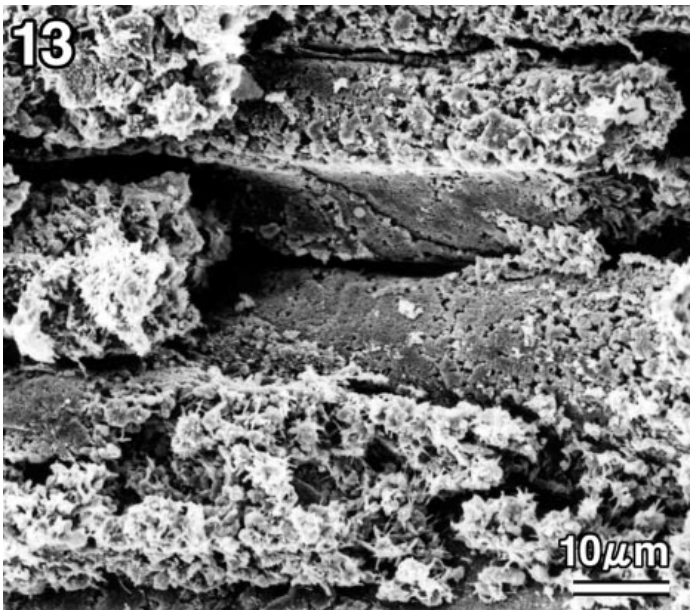

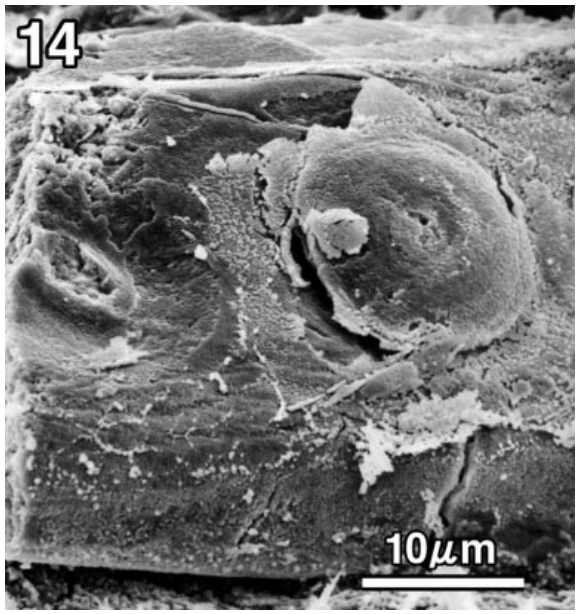

Fig. 13 Sample-**e**. Within each tracheid, the mortar column transformed the texture from diffuse aggregates of burs to fine and dense (from right to left).
Fig. 14 Sample-**e**. The surface of dense and fine mortar molding tracheid lumen was smooth. The wall sculptures such as pit borders and pit cavities were apparently observed with fine texture.

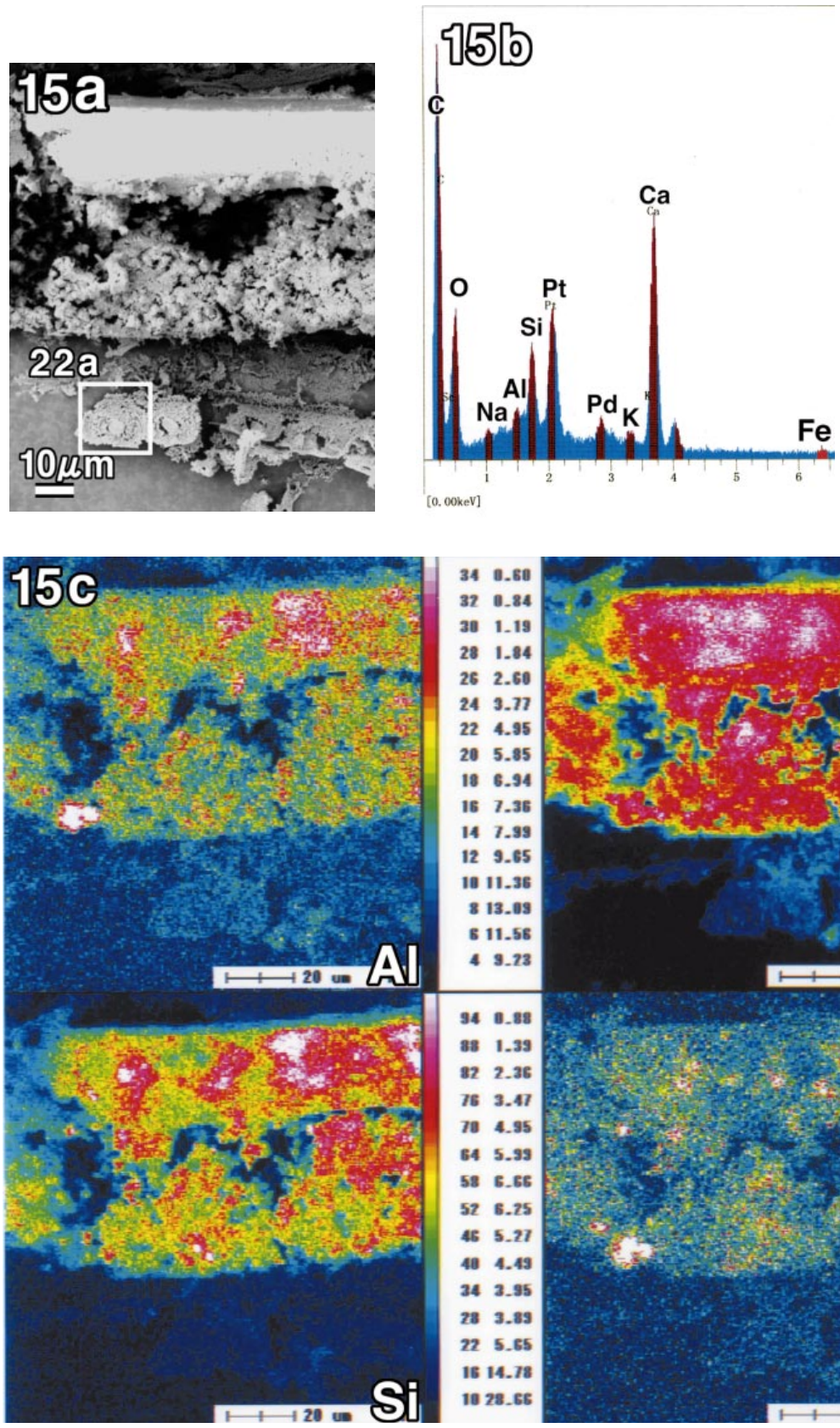

Fig. 15 Sample-f. **15a**: SEI, **15b**: EDS spectrum of the whole area, **15c**: element maps. Three columnar remnants of different types are shown.

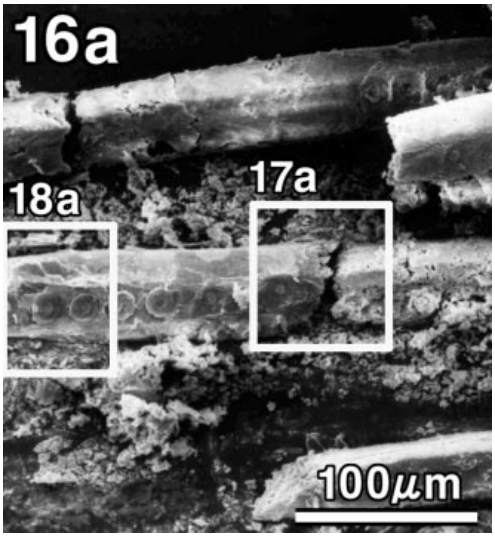

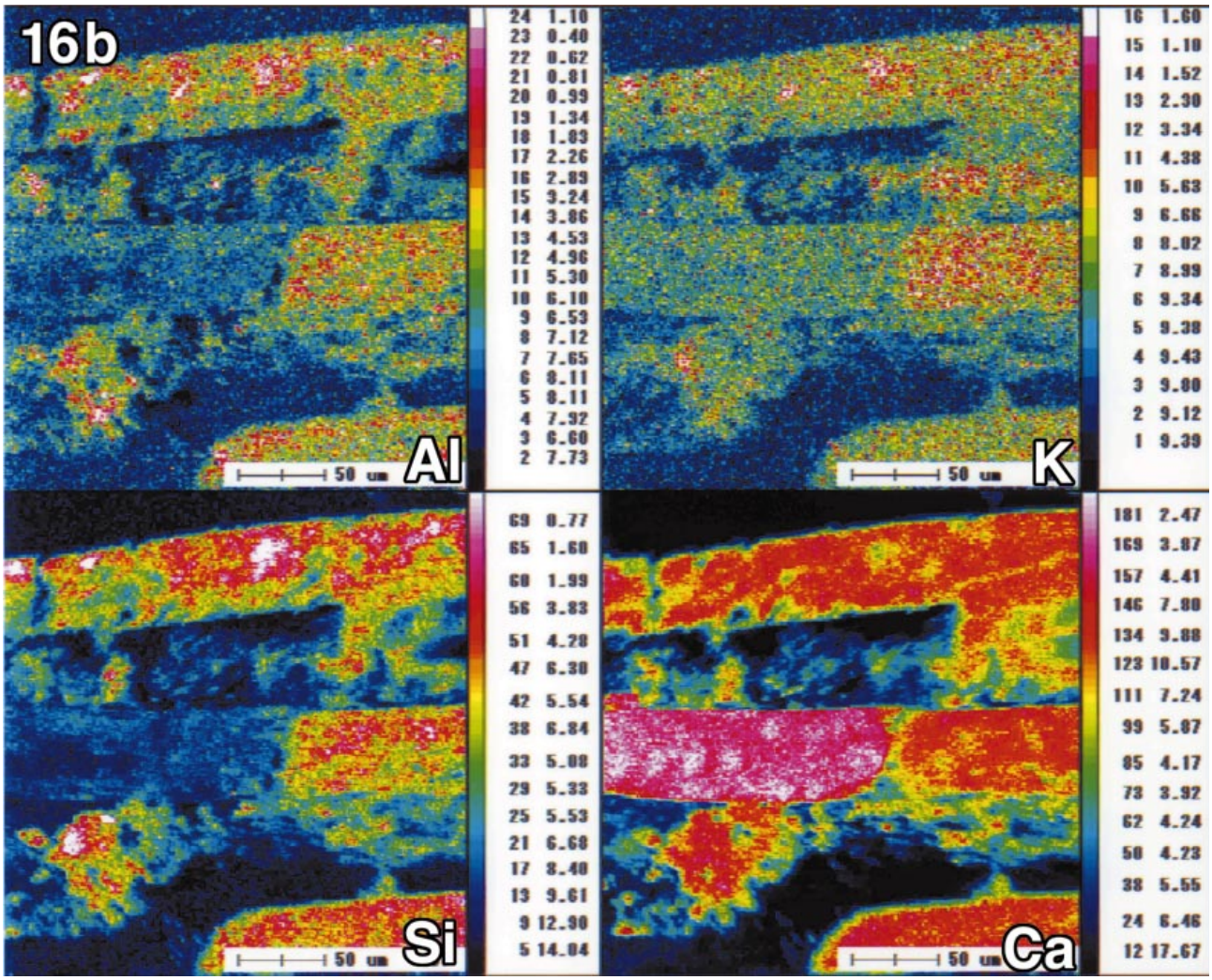

Fig. 16 Sample-**f**. **16a**: SEI, **16b:** element maps. In the area extremely rich in **Ca**, intensities of other elements (**Al**, **Si** and **K**) are apparently very low comparing to other columns.

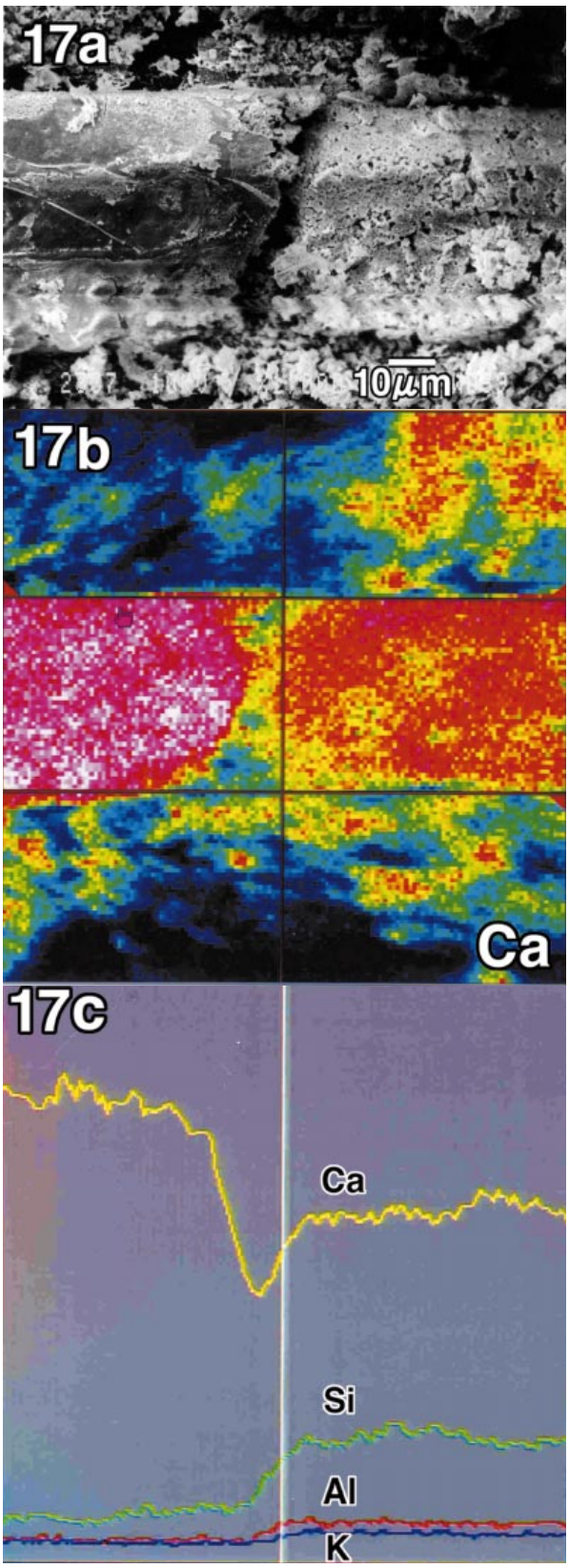

Fig. 17 Sample-**f**. Enlargement of a part of Fig 16a. **17a**: SEI, **17b**: element maps, **17c:** Line profiles indicating the intensity of each element in the area between two horizontal lines in Fig. 17b.

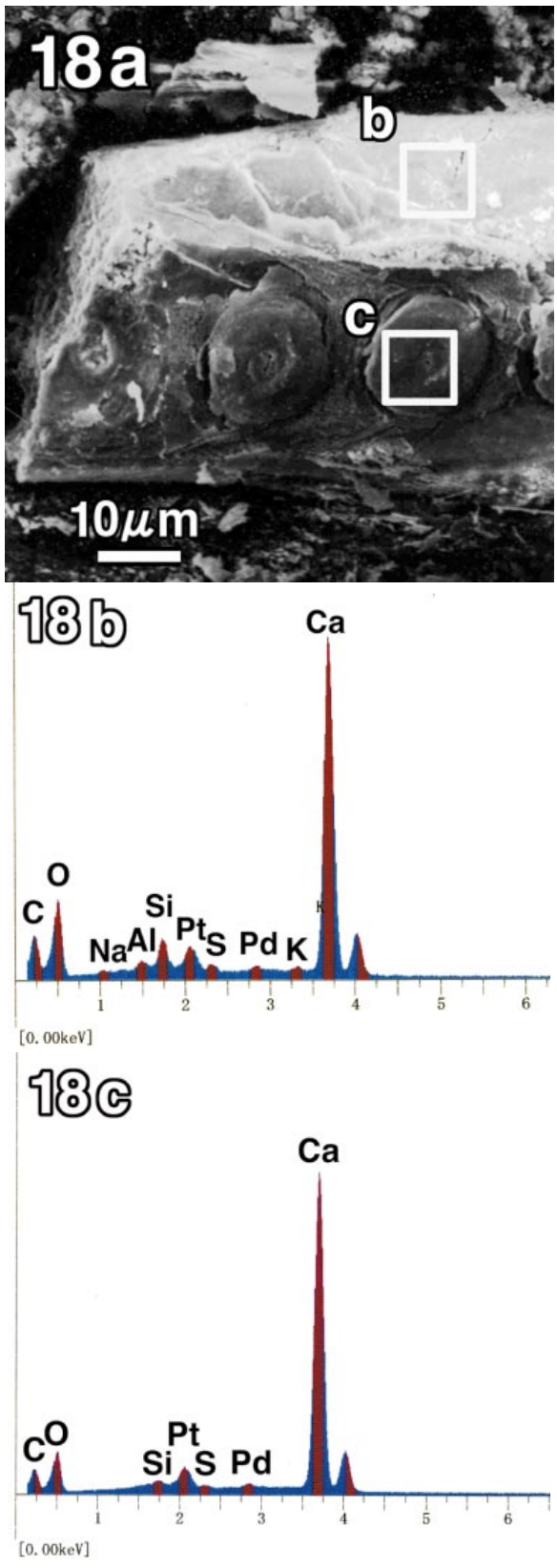

Fig. 18 Sample-**f**. Enlargement of a part of Fig 16a. **18a**: SEI, **18b**: spectrum from the selected area (b), **18c**: EDS spectrum from the mortar molding a pit chamber (c).

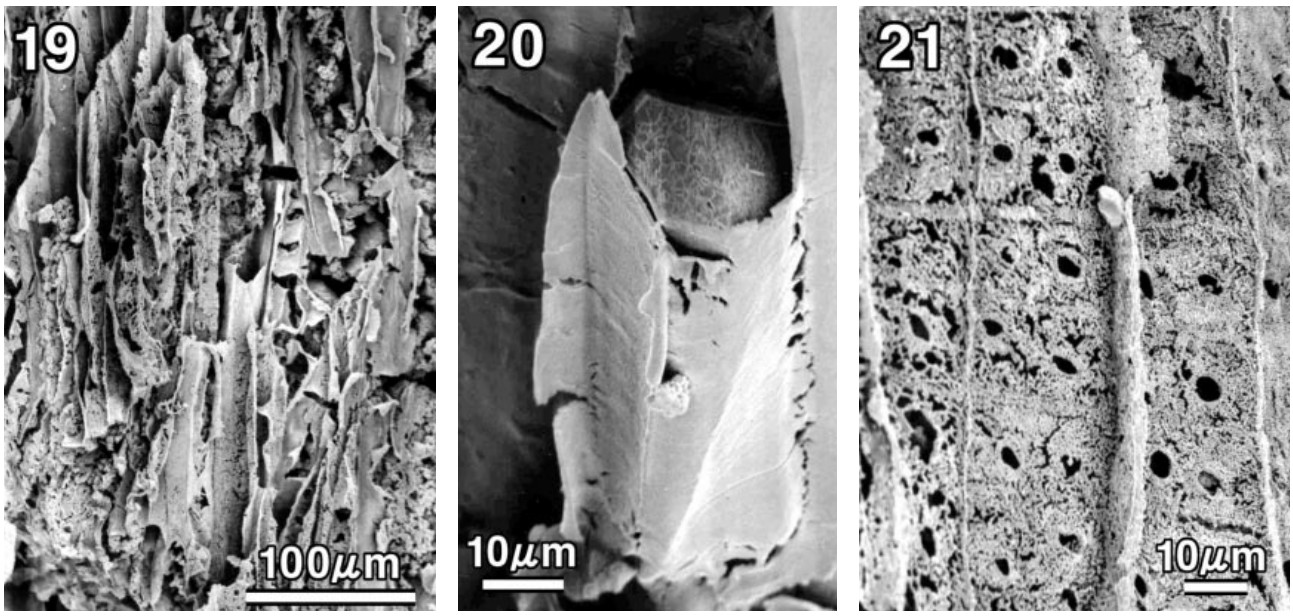

Fig. 19 Sample-**e**. Membranous cinders surround aggregates of grains appearing compound middle lamellae.
Fig. 20 Sample-**e**. Membranous mortar with fine texture completely surrounds a dense columnar mortar.
Fig. 21 Sample-**e**. Membranous mortar with granular texture appears to be radial walls of serial tracheids showing cross-field pitting.

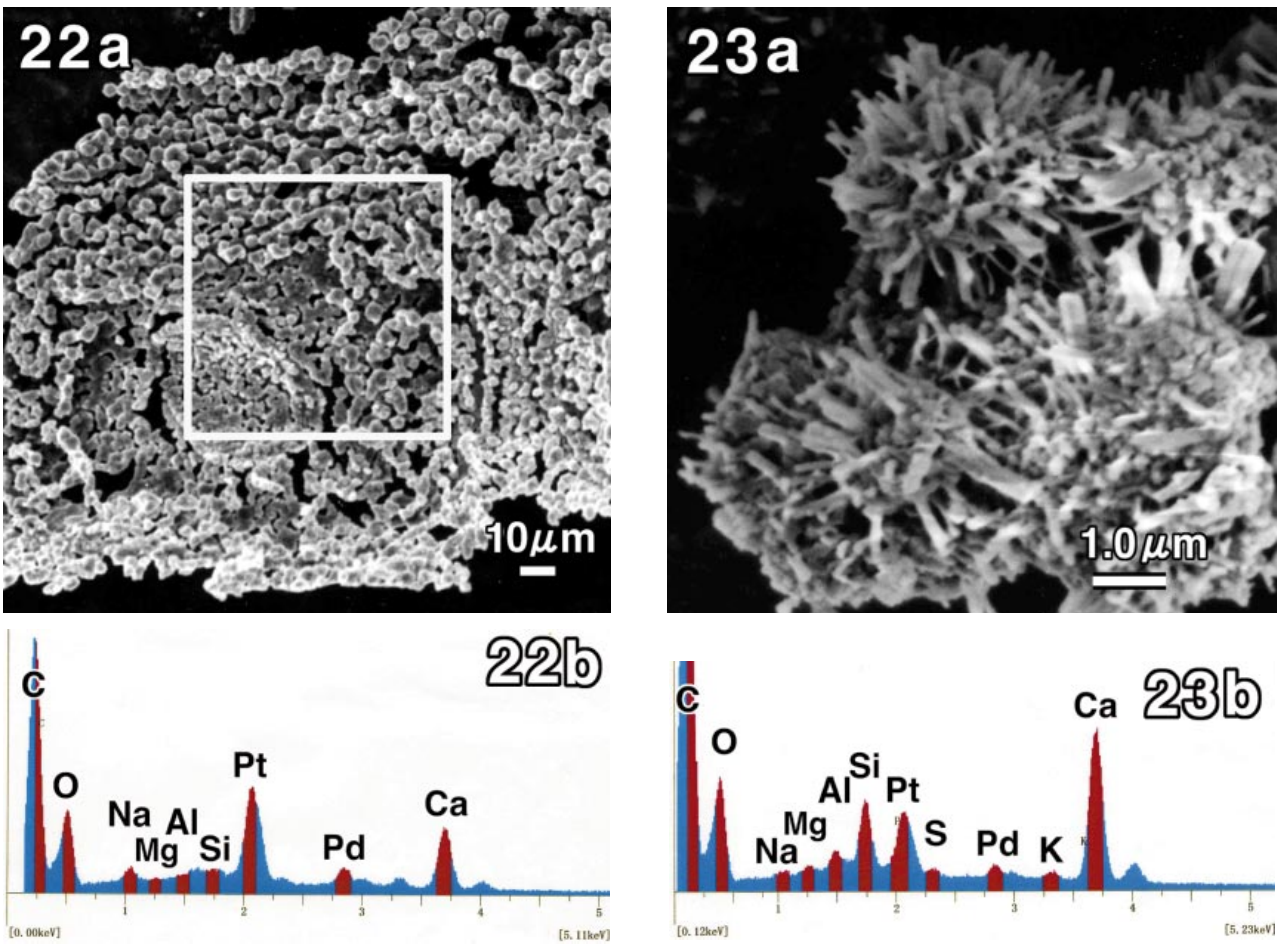

Fig. 22 Sample-**f**. Enlargement of a part of Fig. 15a. Granular membranous mortar with pit structure. **22a**: SEI, **22b**: EDS spectrum from the selected area in Fig. 22a.
Fig. 23 Sample-**f**. Diffuse aggregate of needle-like crystals. **23a**: SEI, **23b**: EDS spectrum.